Progress In Electromagnetics Research Letters, Vol. 70, 99–106, 2017

An Electrically Small Low-Profile and Ultra-Wideband Antenna with Monopole-Like Radiation Characteristics

Hong Zhang*, Fu-Shun Zhang, and Yu-Liang Yang

Abstract—This paper presents an electrically small, low-profile and ultra-wideband antenna with monopole-like radiation type. The antenna is composed of a top-loading hat and two tapered radiation patches on the crossed substrates shorted to the ground. Introducing two tapered radiation patches with the meander loop traces allows for achieving ultra-wideband operation and very low profile simultaneously. In addition, two columns of metal via-holes nested in the crossed substrates can broaden the bandwidth further. The proposed antenna is simulated, fabricated and measured. The measured and simulated results show good agreement and indicate that a measured VSWR lower than 2.0 over 632–3907 MHz (a 144% relative bandwidth) can be accomplished. The antenna has a low profile ($0.053\lambda_{\min}$) in height and occupies a small circle of radius $0.078\lambda_{\min}$, where $\lambda_{\min}$ is the free-space wavelength at the lowest frequency. The antenna has a $k_{\min}a = 0.59$, where $k_{\min}$ is the wavenumber at the lowest frequency of operation. The frequency band covers LTE (0.7 GHz), BDS (1.268 GHz), GPS (1.575 GHz), WIFI (2.5 GHz) and WIMAX (3.5 GHz).

1. INTRODUCTION

With the development of Internet of things and wireless transmission, ultra-wideband (UWB) antenna has been widely applied, especially in military, wireless communication, radar and electronic warfare. UWB technology has the advantages of low cost, high data transfer rate and counteracting the multipath response, which cannot be found in narrow band systems. It is a hot button how to broaden the bandwidth of the antennas to meet the current increasing demand. In fact, the need for broadband antennas with omnidirectional coverage similar to a monopole antenna is increasing. To increase the bandwidth of monopole-type radiators, a lot of methods have been examined. Resistive loading or loading the antenna with loss ferrite material [1, 2] are used. However, the improvements of the bandwidths are obtained at the expense of the antenna gain and radiation efficiency. A variety of printed monopole antennas takes advantages of adding sleeve [3], exploiting a tapered and periodically corrugated edge design on the CPW ground plane [4], adding asymmetric parasitic elements [5], and using anomalous radiation elements such as heart-shaped patch [6] to dramatically improve their bandwidths. However, the profiles of these antennas are relatively high (more than $0.152\lambda_{\min}$, $\lambda_{\min}$ is the free-space wavelength at the lowest frequency).

The antennas applied in aircraft communication suffer from aerodynamic influence. Thus the designed antennas with low profiles are desired. Antennas proposed in [7, 8] ($0.085\lambda_{\min}$ and $0.046\lambda_{\min}$) are low in profile. However, the structures with lumped element matching are complicated. In addition, in order to be mounted in finite space, the antennas should have the lowest $k_{\min}a$ (a is the radius of the smallest Chu' sphere circumscribing the antenna [9]) value.

In this paper, we present an electrically small, low-profile and ultra-wideband antenna with monopole-like radiation pattern. The antenna has an electrical dimension of $0.078\lambda_{\min} \times 0.053\lambda_{\min}$ and achieves an extremely wide frequency band of VSWR less than 2, which exceeds $6.2:1$ octave.

Received 20 July 2017, Accepted 14 September 2017, Scheduled 25 September 2017

* Corresponding author: Hong Zhang (15771938852@163.com).

The authors are with the National Key Laboratory of Antennas and Microwave Technology, Xidian University, Xi'an 710071, China.

2. ANTENNA STRUCTURE

The low profile and bandwidth improvement of a conventional monopole antenna can be obtained by two approaches: first, top-loading with a capacitive plate and second, coupled sectorial loop antenna (CSLA [20]) with shorting traces. In this paper, the aforementioned two approaches are combined to design a low-profile and UWB antenna.

Figure 1 shows the general view and exploded view of the three-dimensional topology of the antenna. The structure is composed of a circular top-loading hat, two crossed substrates and ground as shown in Figure 1(b). The tapered patches and meander lines are printed on the two crossed substrates. In addition, four oblique slots and four crescent slots are etched on the patches and meander lines, respectively, which are used to improve the impedance matching. Here, the meander lines connected to the tapered patches are shorted to the ground. As shown in Figure 1(b), loop traces based on CSLA are composed of the bevel edges of the tapered patches, meander lines and ground. In this design, the loop traces are used to broaden the bandwidth and realize miniaturization. For two crossed substrates, two complementary slender parts are separately cut from the middle of the two substrates. This results in disconnected tapered patches. Therefore, one column of metalized via-holes in each of the two crossed substrates is introduced. Metalized via-holes in one substrate are welded to the tapered patch on the other substrate to guarantee the current's breakover. Finally, there are grooves grubbed in the top-loading hat and the ground. The proposed antenna is fixed by the two crossed substrates nested within the grooves to ensure the two crossed substrates orthogonal. All the substrates used are FR4 with a relative permittivity of 4.4, dielectric loss tangent of 0.02 and thickness of 1 mm.

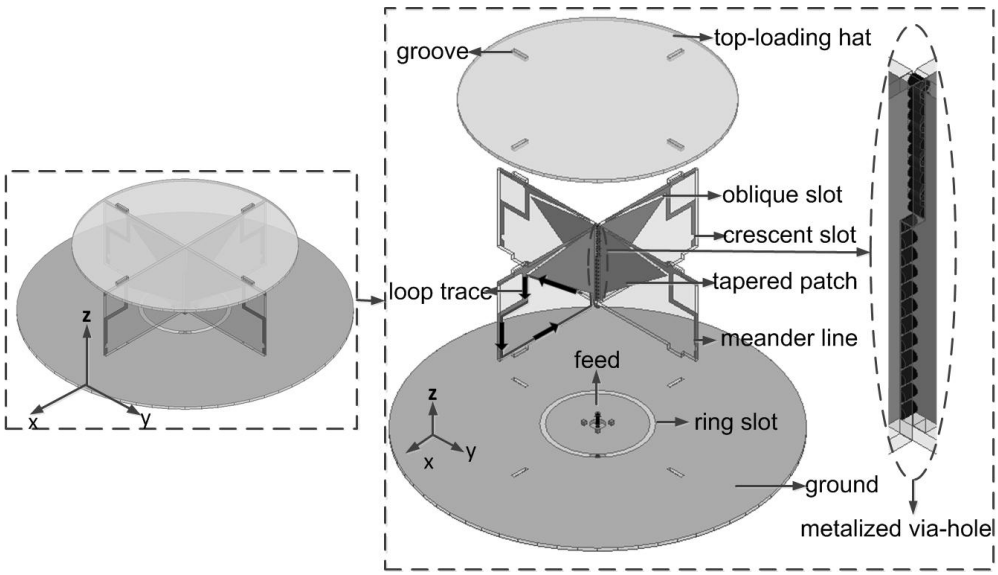

Figure 1. Three-dimensional topology of the antenna. (a) General view. (b) Exploded view.

Figure 2 shows the side view and top view of the geometry of the antenna. h is the height of the two crossed substrates. The meander line has the length of $h + l2$ and width of $w2$. The radius of the ground R_g equals 160 mm. R_p is the radius of the top-loading hat. Additionally, $r1$ and $r2$ are the inter and outer radii of the ring slot, respectively.

Simulations are performed using the HFSS (High Frequency Structure Simulator) software. The size details of the antenna are shown in Table 1. The two crossed substrates are identical except for the positions of via-holes, so only one crossed substrate size is given as shown in Figure 2.

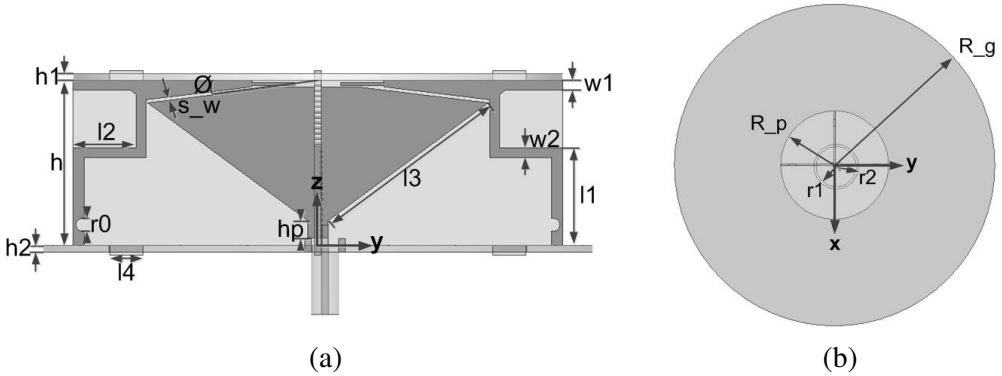

(a) (b)

Figure 2. Geometry of the antenna. (a) Side view. (b) Top view.

Table 1. Antenna dimension (unit: mm).

h	$h1$	$h2$	hp	$l1$	$l2$	$l3$	$l4$
25	1	1	2.6	14.7	9.6	30.1	5
s_w	$w1$	$w2$	$\Phi(deg)$	$r0$	$r1$	$r2$	R_p
0.5	1.5	1.5	3	1	13.8	15.3	37

3. KEY STRUCTURE AND PARAMETRIC STUDY

3.1. Key Structure

3.1.1. Meander Shorting Traces

In this paper, the effective current paths of the antenna is extended by adding meander shorting traces. To prove this, current distributions on one of tapered radiation patches at 0.9 GHz, 1.8 GHz, 3.6 GHz are given in Figure 3.

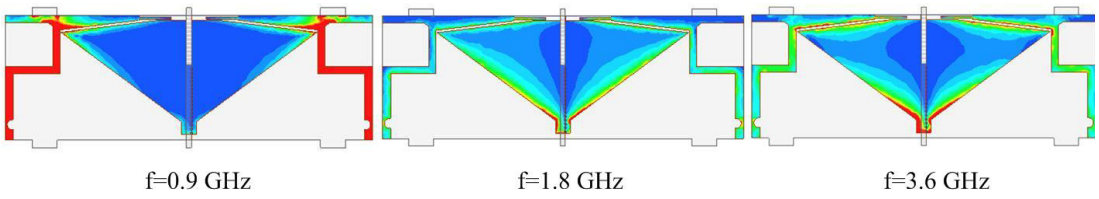

Figure 3. Current distribution on the antenna at 0.9 GHz, 1.8 GHz, 3.6 GHz.

Figure 3 shows that at 0.9 GHz, the electric current density is very strong on the meander shorting traces. Therefore, it is proved that the low-frequency operation of the antenna is attributed to the meander shorting traces. However, the currents at 1.8 GHz and 3.6 GHz become much weaker, indicating that they no longer act as the main radiation parts. As a matter of fact, at high frequencies, the antenna derives the radiation mainly from the two tapered patches near the feed structure. And the resonant lengths are corresponding to $\lambda_s/4$ (20 mm at 1.8 GHz, 10 mm at 3.6 GHz) (λ_s is the guide wavelength on the substrate). Multi-resonance performance results in the UWB performance of the antenna.

To further illustrate the effectiveness of the meander lines, Figure 4(a) gives simulated VSWRs of the antennas with meander lines and straight lines. It is obviously shown that meander lines not only improve the whole impedance matching but also broaden the bandwidth.

3.1.2. Metalized Via-holes

According to the above analysis, antenna dimensions near the feed structure have a significant effect on the performance at high frequencies (HF). However, to realize the crossed structure of the two substrates, two complementary slender parts are separately cut from the middle of the two substrates. This leads to the downward shift of the HF. To solve the problem, we introduce metalized via-holes to guarantee the current's breakover. The comparison results of the antenna with/without via-holes are shown in Figure 4(b). Figure 4(b) reveals that the addition of metalized via-holes contributes to the improvement of the impedance matching at the HF band.

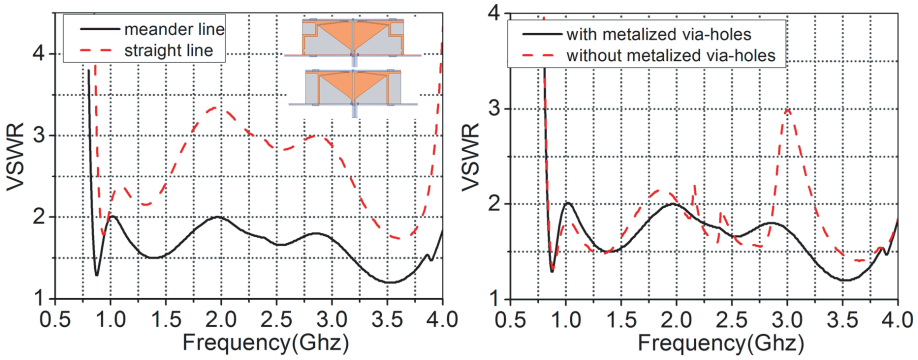

Figure 4. Simulated VSWRs. (a) of loading meander lines and straight lines, (b) of the antenna with/without metalized via-holes.

3.2. Parametric Study

The proposed antenna has three key parameters, namely, the height h of the crossed substrates, the radius R_p of the top-loading hat and the width $w2$ of the meander line. The effect of these parameters on the VSWRs of the proposed antenna is studied. When one parameter is changed, the other parameters are fixed as shown in Table 1.

The first parameter is the meander line width $w2$. Figure 5(a) shows the variations of VSWR with frequency for the meander line width $w2 = 1.25$ mm, 1.45 mm and 1.65 mm. It is shown that increasing the meander line width can improve the VSWR of the low frequencies, but the middle frequencies does not match well. As a tradeoff, the optimal value of the meander line width $w2$ is selected as 1.45 mm.

The second parameter is the top-loading patch radius R_p. Figure 5(b) shows the variations of VSWR with frequency for the top-loading patch radius $R\_p = 35$ mm, 37 mm and 39 mm. Decreasing

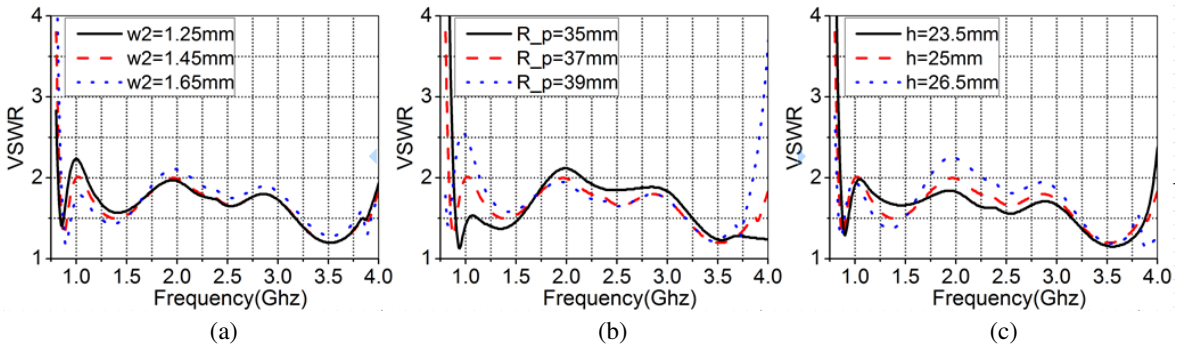

Figure 5. Variations of VSWRs with frequency for different parameters. (a) Meander lines width $w2$, (b) top-loading patch radius R_p, (c) crossed substrates' height h.

the top-loading patch radius can improve the VSWR of the low frequencies and high frequencies, but the middle frequencies does not match well. Therefore, the optimal value of the top-loading patch radius R_p is chosen as 37 mm.

The third parameter is the crossed substrates' height h. Figure 5(c) shows the variations of VSWR with frequency for the crossed substrates' height $h = 23.5$ mm, 25 mm and 26.5 mm. It is observed that, with the decreasing of h, the input impedance of middle frequency band is well matched. Nevertheless, the antenna at the high frequencies matches poorly. Hence, the crossed substrates' height h is used at 25 mm after the optimization.

Finally, the antenna is optimized with the HFSS carefully. And the obtained optimal size of the proposed antenna is shown in Table 1.

4. SIMULATED AND MEASURED RESULTS

Based on the above analysis, the proposed antenna is fabricated and measured. Figure 6 shows a photograph of the measured antenna in an anechoic chamber. The antenna is composed of four 1-mm thick FR4 substrates and fed with a 50-Ω SMA connector.

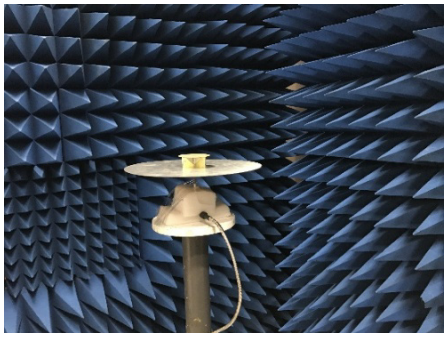

Figure 6. Photograph of the antenna prototype.

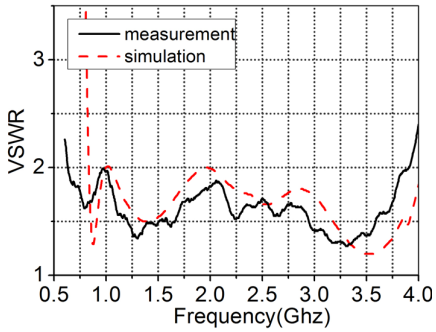

Figure 7. Simulated and measured VSWR.

The measured and simulated results of VSWR are simultaneously shown in Figure 7 for a striking contrast. It is obviously observed that the measured result agrees well with the simulated one. It is noted that the lowest operating frequency is shifted downward. In practice, the actual dielectric materials are inhomogeneous, and there are discontinuities of welding part between the SMA connector and feed-line, which will influence the VSWR. Another factor is soldering tin used in jointing substrates. All factors may result in the difference between simulated and measured results.

Figure 8 shows the simulated and measured normalized radiation patterns of the antenna at 0.9 GHz, 1.8 GHz and 3.6 GHz. It is observed that the antenna has a good monopole-like radiation characteristic in the whole band. It is noted that the maximum radiation direction is in the upper half space due to the big ground. In addition, the simulated radiation patterns agree well with the measured ones.

The simulated and measured gains and simulated radiation efficiency of the antenna are shown in Figure 9. The measured gain varies between 1.5 dBi and 5.6 dBi, and the simulated gain varies in the range of −4.5–6.12 dBi within the operating frequency band from 0.632 GHz to 3.907 GHz. It is noted that the simulated gain at the low frequency is significantly decreased compared to the measured one. This is because the operating band of the fabricated antenna shifts to the lower band. It can be observed that the simulated efficiency of the antenna is over 95% within most operating bandwidth.

Table 2 presents a comparison between the performance of the proposed antenna and some compact, broadband antennas reported in the references.

Table 2 shows a distinct comparison between previous designs with the monopole-like radiation characteristics and this paper, where Φ is the diameter of the antennas, and $\lambda_{\min}$ is the free-space wavelength at the lowest operating frequency. In this table, structure denotes the antenna outline; VSWR means the lowest value of VSWR within the reported bandwidth; BW signifies the relative

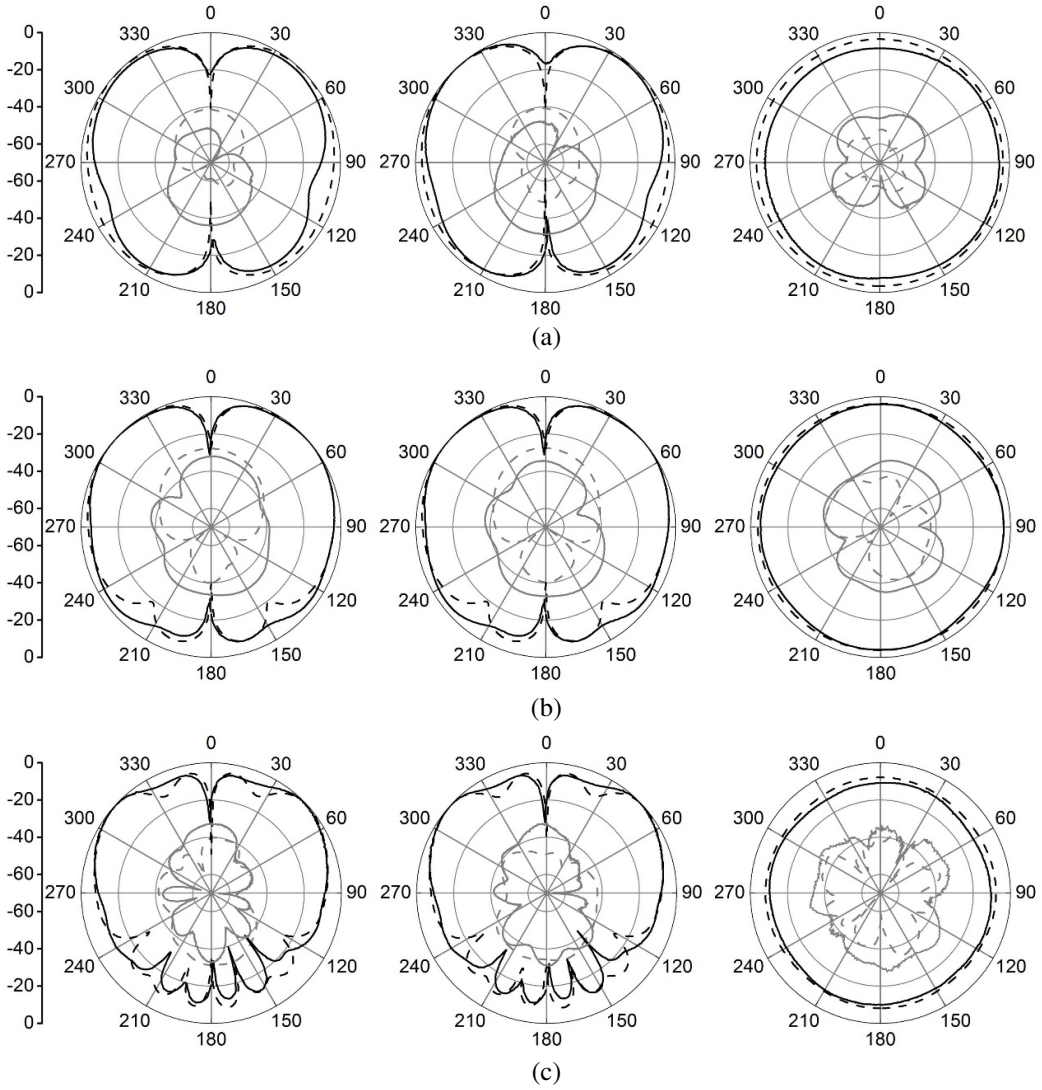

Figure 8. Simulated and measured normalized radiation pattern results of the proposed antenna for the xz (left) plane, yz (middle) plane and xy (right) plane at (a) 0.9 GHz. (b) 1.8 GHz. (c) 3.6 GHz. The black solid line is the measured co-pol, the black dashed line is the simulated co-pol, the gray solid line is the measured cross-pol, and the gray dashed line is the simulated cross-pol. (a) $f = 0.9$ GHz. (b) $f = 1.8$ GHz. (c) $f = 3.6$ GHz.

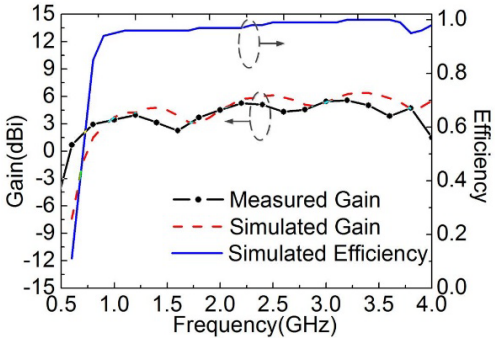

Figure 9. Simulated and measured gains and efficiency of the antenna.

Table 2. Performance comparison between this work and filters in other papers.

Ref.	Structure	Dimensions ($\lambda^1_{\min}$)	VSWR	Operation band (GHz)	BW (%)	$k^2_{\min}a^3$
[10]	cylinder	Φ 0.38 × 0.16	2.2	1.7–14.5	158	1.56
[11]	cylinder	Φ 0.4 × 0.094	2.0	0.47–6.0	171	1.39
[12]	cylinder	Φ 0.283 × 0.072	1.93	2.15–14	147	1.01
[13]	cylinder	Φ 0.52 0.07	2.0	1.5–7.8	135	1.69
[14]	cylinder	Φ 0.165 × 0.075	3.0	0.225–0.4	56	0.7
[15]	cube	0.2 × 0.2 × 0.067	2.0	1.83–2.7	38	0.98
[16]	cylinder	Φ 0.424 × 0.079	1.93	4.03–11.0	93	1.42
[17]	cube	0.204 × 0.204 × 0.087	1.93	3.06–12.0	119	1.06
[18]	cube	0.208 × 0.208 × 0.068	1.93	0.8–2.3	97	1.02
[19]	sphere	Φ 0.192	2.0	0.576–2.985	135	0.6
paper	cylinder	Φ 0.156 × 0.053	2.0	0.632–3.9	144	0.59

[1] $\lambda_{\min}$ is the free-space wavelength at the lowest frequency of operation.
[2] $k_{\min}$ is the wavenumber at the lowest frequency of operation of the antenna.
[3] a is the radius of the smallest Chu' sphere circumscribing the antenna.

bandwidth. BWs of the antennas in [10–12] are superior to that of the antenna in this paper, but the $k_{\min}a$ values are relatively inferior. In [19], the antenna's $k_{\min}a$ is similar to that of the proposed antenna, but BW is 9% less than that in this paper. The proposed antenna excels the antennas in other references in both $k_{\min}a$ and BW. Furthermore, the designed antenna has lower profile and smaller top-loading hat than the antennas in other references.

5. CONCLUSION

An electrically small, low-profile, ultra-wideband antenna with monopole-like radiation type is presented. The antenna is composed of a top-loading hat, two crossed substrates and a ground plane. The top-loading hat and the meander lines on the two crossed substrates are introduced to broaden the bandwidth and realize the miniaturization of the antenna, respectively. The antenna is simulated, fabricated and measured. The antenna operates in a wide frequency band from 632 MHz to 3907 MHz, namely a 144% relative bandwidth. The antenna size is $\Phi 0.156\lambda_{\min} \times 0.053\lambda_{\min}$ ($\lambda_{\min}$ is the free-space wavelength at the lowest frequency). Simulated and measured results show that the antenna has good performance. The frequency band covers LTE (0.7 GHz), BDS (1.268 GHz), GPS (1.575 GHz), WIFI (2.5 GHz) and WIMAX (3.5 GHz), so the antenna design is of practical value for the ultra-wideband system.

REFERENCES

1. Yu, Y. K. and J. Li, "Analysis of electrically small size conical antennas," *Progress In Electromagnetics Research Letters*, Vol. 1, 85–92, 2008.
2. Moon, H., G.-Y. Lee, C.-C. Chen, and J. L. Volakis, "An extremely low profile ferrite-loaded wideband VHF antenna design," *IEEE Antennas and Wireless Propagation Letters*, Vol. 11, 322–325, 2012.
3. Chen, H.-D., H.-M. Chen, and W.-S. Chen, "Planar CPW-fed sleeve monopole antenna for ultra-wideband operation," *IEEE Transaction on Antennas and Propagation*, Vol. 152, No. 6, Dec. 2005.
4. Chen, N.-W. and Y.-C. Liang, "An ultra-wideband, coplanar-waveguide fed circular monopole antenna with improved radiation characteristics," *Progress In Electromagnetics Research C*, Vol. 9, 193–207, 2009.

5. Sugimoto, S. and H. Iwasaki, "Wide band planer monopole antenna with asymmetric parasitic elements," *IEEE Conference Publication*, 1–4, 2010.
6. Hua, C., Y.-L. Lu, and T. J. Liu, "UWB heart-shaped planar monopole antenna with a reconfigurable notched band," *Progress In Electromagnetics Research Letters*, Vol. 65, 123–130, 2017.
7. Amin, S. M., M. H. Abadi, and N. Behdad, "An electrically small, vertically polarized ultra-wideband antenna with monopole-like radiation characteristics," *IEEE Antennas and Wireless Propagation Letters*, Vol. 13, 2014.
8. Ghaemi, K. and N. Behdad, "A low profile, vertically polarized ultra wide band antenna with monopole-like radiation characteristics," *IEEE Transactions on Antennas and Propagation*, Vol. 63, No. 8, Aug. 2015.
9. Chu, L. J., "Physical limitations of omni-directional antennas," *Journal of Applied Physics*, Vol. 19, 1163, 1948.
10. Behdad, N. and K. Sarabandi, "A compact antenna for ultra-wideband applications," *IEEE Transactions on Antennas and Propagation*, Vol. 53, No. 7, Jul. 2005.
11. Zhou, S., J. Ma, J. Deng, and Q. Liu, "A low-profile and broadband conical antenna," *Progress In Electromagnetics Research Letters*, Vol. 7, 97–103, 2009.
12. Oh, J. and K. Sarabandi, "Ultra-wideband, miniaturized, low profile, omnidirectional antenna using a novel reactive loading approach," *IEEE Antennas and Propagation Society International Symposium (APSURSI)*, 2012.
13. Yang, L., Z.-Y. Zhang, G. Fu, Y.-X. Zhang, and Y. Li, "A novel low-profile quadripod kettle antenna with enhanced bandwidth," *Progress In Electromagnetics Research Letters*, Vol. 144, 241–247, 2014.
14. Luo, D., X. Zhou, J. Li, and X. Xuan, "A novel low profile UWB monopole antenna," *2016 Progress In Electromagnetic Research Symposium (PIERS)*, Shanghai, China, Aug. 8–11, 2016.
15. Nakano, H., H. Iwaoka, K. Morishita, and J. Yamauchi, "A wideband low-profile antenna composed of a conducting body of revolution and a shorted parasitic ring," *Progress In Electromagnetics Research Letters*, Vol. 56, No. 4, Apr. 2008.
16. Zurcher, J.-F., "A vertically polarized antenna with 90% bandwidth," *Microwave and Optical Technology Letters*, Vol. 55, No. 3, Mar. 2013.
17. Koohestani, M., J.-F. Zürcher, A. A. Moreira, and A. K. Skrivervik, "A novel, low-profile, vertically-polarized UWB antenna for WBAN," *IEEE Transactions on Antennas and Propagation*, Vol. 62, No. 4, Apr. 2014.
18. Nguyen-Trong, N., A. Piotrowski, T. Kaufmann, and C. Fumeaux, "Low-profile wideband monopole UHF antennas for integration onto vehicles and helmets," *IEEE Transactions on Antennas and Propagation*, Vol. 64, No. 6, Jun. 2016.
19. Li, M. and N. Behdad, "A compact, capacitively fed UWB antenna with monopole-like radiation characteristics," *IEEE Transactions on Antennas and Propagation*, Vol. 65, No. 3, Mar. 2017.
20. Elsherbini, A. and K. Sarabandi, "Very low-profile top-loaded UWB coupled sectorial loops antenna," *IEEE Transactions on Antennas and Propagation*, Vol. 10, 2011.